Conformational and Environmental Effects on the Electronic and Vibrational Properties of Dyes for Solar Cell Devices

Edoardo Buttarazzi,[1,2] Antonio Inchingolo,[3] Danilo Pedron,[3] Marta Erminia Alberto,[4] Elisabetta Collini,[3] and Alessio Petrone[2,1,5]

[1)]*Scuola Superiore Meridionale, Largo San Marcellino 10, I-80138, Napoli, Italy*

[2)]*Department of Chemical Sciences, University of Napoli Federico II, Complesso Universitario di Monte S. Angelo, via Cintia 21, I-80126, Napoli, Italy*

[3)]*Department of Chemical Sciences, University of Padova, via Marzolo 1, I-35131, Padova, Italy*

[4)]*Department of Chemical and Chemical Technologies, University of Calabria, via Pietro Bucci ed. 12/C, I-87036, Arcavacata di Rende, Cosenza, Italy*

[5)]*Istituto Nazionale Di Fisica Nucleare, sezione di Napoli, Complesso Universitario di Monte S. Angelo ed. 6, via Cintia, I-80126, Napoli, Italy*

(*Electronic mail: marta.alberto@unical.it, elisabetta.collini@unipd.it, alessio.petrone@unina.it)

(Dated: 3 May 2024)

The main challenge for solar cell devices is harvesting photons beyond the visible by reaching the red-edge ($650-780\,\mathrm{nm}$). Dye-sensitized solar cell (DSSC) devices combine the optical absorption and the charge separation processes by the association of a sensitizer as a light-absorbing material (dye molecules, whose absorption can be tuned and designed) with a wide band gap nanostructured semiconductor. Conformational and environmental effects (i.e. solvent, pH) can drastically influence the photophysical properties of molecular dyes. This study proposes a combined experimental and computational approach for the comprehensive investigation of the electronic and vibrational properties of a unique class of organic dye compounds belonging to the family of red-absorbing dyes, known as squaraines. Our focus lies on elucidating the intricate interplay between the molecular structure, vibrational dynamics, and optical properties of squaraines using state-of-the-art density functional theory (DFT) calculations and spectroscopic techniques. Through systematic vibrational and optical analyses, we show that (i) the main absorption peak in the visible range is influenced by the conformational and protonation equilibria; (ii) the solvent polarity tunes the position of the UV-Vis absorption, and (iii) the vibrational spectroscopy techniques (infrared and Raman) can be used as informative tools to distinguish between different conformations and protonation states. This comprehensive understanding offers valuable insights into the design and optimization of squaraine-based DSSCs for enhanced solar energy conversion efficiency.

I. INTRODUCTION

The pursuit of green, efficient, and cost-effective solar energy conversion has spurred the exploration of diverse materials for more efficient photovoltaic technologies.[1–8] Until now, the photovoltaic field has been ruled by usually rather expensive inorganic solid-state junction devices.[9,10] Among the several alternatives recently proposed and available, dye-sensitized solar cells (DSSCs) are becoming prominent.[11–13] The key idea of DSSC devices is to combine the visible light absorption and the charge separation processes by the association of a sensitizer as a light-absorbing material (dye molecules interacting with the semiconductor surface, responsible for the light absorption in the device) with a wide band gap nanostructured semiconductor (not significantly contributing to the solar light absorption).[2,11,13] Solar light induces charge-separation (exciton formation) that can be injected (electron injection) into a substrate (usually TiO_2 and ZnO-based DSSCs).[11,14] The main challenge for all solar cell devices is the possibility of obtaining photon harvesting beyond the visible by reaching the red-edge ($650-780$ nm) or the near-infrared (NIR, $780-2500$ nm) wavelength region, which accounts for over half of the solar energy reaching the Earth's surface.[2,15] Despite the scientific and economic efforts, harvesting light beyond the visible region is not a reality yet.[13,16,17] For photoactive materials with a typical film thickness for which high structural quality is obtained, the main problem is that the ability to capture photons is lower in the range of $600\,\text{nm} < \lambda < 780\,\text{nm}$ compared to shorter wavelengths. This is because the efficiency of exciton formation rapidly decreases for red frequencies.[18] In DSSCs, the sensitizer dye plays a crucial role in this quest, since its absorption can be tuned and designed for initiating the electron injection into the conduction band of the semiconductive material.[2,13,17] Various molecular sensitizers, including chlorophylls[19–22], anthocyanins[22,23], metal-based complexes[14,24,25], and carbazole-based compounds[26–28], have been explored. However, optimizing the spectral response of DSSCs, particularly in the red region of the electromagnetic spectrum, remains a key focus for enhancing the overall efficiency.[13,17]

This study centers on a unique class of red-absorbing organic dye compounds belonging to the family of squaraines.[29–32] Such molecules are synthesized through electrophilic aromatic substitution of electron-rich derivatives and squaric acid, giving access to a variety of symmetric and asymmetric structures with easily tunable optical characteristics, such as the visible light absorption.[29,30,33–35] Despite the large amounts of experimental works and proposed applications, a thorough understanding of their complex photophysics is still limited by practical and

conceptual difficulties, from both experimental and computational points of view. Prototypical squaraine-based DSSCs suffer from a low power conversion efficiency[13,17] and there is a wide margin to tune their crucial photophysical properties. Several studies have pointed out the crucial role of quadrupolar interaction, aggregate formations, and vibronic couplings on the optical properties on this class of molecules.[36–38] In the past decades, the scientific community mostly focused on improving the quantum yield and overall DSSC performances, neglecting the effects of conformational and acid-base equilibria on their properties, which are instead important features to acquire an in-depth characterization of such dyes. Therefore, this work aims to provide a detailed exploration of the electronic and vibrational properties of selected squaraines by an accurate experimental-computational protocol, to gain deeper insights into their fascinating photophysics.

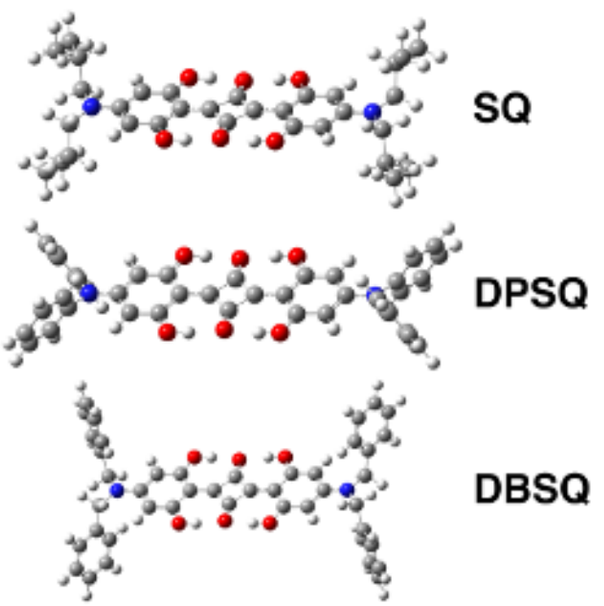

FIG. 1. B3LYP/6-31+G(d,p)/C-PCM minimum energy structures in acetonitrile solution of **SQ**, **DPSQ** and **DBSQ** dyes. Atoms color palette: C-dark gray; H-white; N-blue; O-red.

Specifically, we focus on three prototypical squaraine molecules commercially available and largely employed: 2,4-Bis[4-(N,N-diisobutylamino)-2,6-dihydroxyphenyl]squaraine (**SQ**), 2,4-Bis[4-(N,N-diphenylamino)-2,6-dihydroxyphenyl]squaraine (**DPSQ**), and 2,4-Bis[4-(N,N-dibenzylamino)-2,6-dihydroxyphenyl]squaraine (**DBSQ**) (see Figure 1), providing a careful analysis of their electronic (UV-Vis) and vibrational (infrared and Raman) spectra. We wish to stress that several factors, such as the choice of the solvent and thermal fluctuations, can play a pivotal role in perturbing the conformations and intramolecular hydrogen bond network. Protic solvents,

i.e. methanol, or acid base equilibria, i.e. mono-anionic species, can promote a molecular distortion from their planar conformations, leading to changes in the electronic and vibrational spectra in the studied squaraines. The reduction of intramolecular hydrogen bond interactions indicates a significant alteration in the internal forces that stabilize the planar molecular structure. A key feature of this distortion is the rotation or twisting of the C–C bonds between the squaric and phenolic carbon atoms. Such kind of analysis is extremely important to design next-generation squaraines with improved efficiency. Indeed, a full knowledge of the electronic structure, vibrational motions, conformational and acid-base speciation is a basic requirement before proceeding with rational structural modifications aimed to reach better performances.

Density functional theory (DFT) was here employed for the *ab initio* treatment and molecular interpretation of electronic and vibrational properties, since it has an optimal balance between accuracy and computational cost and it has been vastly employed for the characterization of both vibrational/dynamical properties of molecules[39–41] and the description of the electronic structure of both the ground and excited electronic states in materials and biological systems.[42–54] Once we have established the most accurate theory level for our investigations, we further analyzed the electronic and vibrational properties of planar, distorted, and monoanionic squaraines. Raman and infrared (IR) spectroscopies were employed to scrutinize the vibrational modes associated with these different structural configurations. These vibrational analyses provided valuable insights into the molecular motions and structural dynamics of squaraines in each conformation. Absorption spectra (also in different solvents) were systematically measured and computed for each conformation and protonation state. While previous studies underlined the importance of accounting for vibronic couplings to interpret the absorption lineshapes in the experimental spectra,[55] our calculations also suggested the presence of an additional layer of complexity given the role of conformational fluctuations and protonation states that could partially contribute to the experimental spectra as well. These findings are crucial for future advanced spectroscopic characterization of nonlinear and transport properties of squaraines.

II. MATERIALS AND METHODS

A. Experimental Details

2,4-Bis[4-(N,N-diisobutylamino)-2,6-dihydroxyphenyl]squaraine (**SQ**), 2,4- Bis[4-(N,N-diphenylamino)-2,6-dihydroxyphenyl]squaraine (**DPSQ**), and 2,4-Bis[4-(N,N-dibenzylamino)-2,6-dihydroxyphenyl]squaraine (**DBSQ**) were purchased from Merck and used without further purification. UV-Vis spectra were recorded on sample solutions prepared by dissolving a suitable amount of squaraine powders in spectroscopic-grade anhydrous solvents. The presence of aggregates in the adopted conditions has been excluded, verifying that the lineshape of the absorption bands does not significantly vary after dilution of at least two orders of magnitude. The weak signal at about 720 nm is caused by a solvent impurity. Infrared spectra were recorded on powders dispersed in KBr pellets. Raman spectra were recorded on squaraine powders pressed onto KBr pellets with a home-built micro-Raman system, based on a Triax-320 ISA spectrograph, equipped with a holographic 1800 g/mm grating and a CCD detector (Horiba Scientific Symphony II FIOE). The excitation source was a Spectra Physics Ar^+ laser operating at 514.5 nm. An Olympus BX 40 optical microscope equipped with a long working distance 20x / 0.40 objective was optically coupled to the spectrograph. The Raman spectra were recorded between 80 and 4000 cm^{-1} and with an instrumental resolution of about 2 cm^{-1}. To avoid optical damage, readily occurring at room temperature, the sample was held in a cryostat cell (Linkam Scientific Instruments) at 100 K and the power of the exciting radiation was maintained between 0.1 and 0.5 mW.

B. Computational Details

All systems were treated at DFT level of theory and all calculations were performed through the commercial Gaussian 16, version C.01, suite of programs.[56] Electronic structure calculations were performed by solving the Kohn-Sham equation using the following functionals: the global hybrid Becke 3-parameter Lee-Yang-Parr, B3LYP,[57–59] the hybrid version of the Perdew-Burke-Ernzerhof functional, PBE0,[60] the Minnesota hybrid functionals M06[61] and M06-2X,[61] the long-range-corrected version of B3LYP using the Coulomb-attenuating method, CAM-B3LYP,[62] and the range-separated hybrid functional of Heyd-Scuseria-Ernzerhof, HSE06,[63–69] in combination with the 6-31+G(d,p) basis set[70–81] (see Results and Discussion section for other tested basis sets). Solvent effects were taken into account by employing implicit solvation models, in particular in

this study was used the conductor-like polarizable continuum model (C-PCM).[82–87] Investigated solvents are acetonitrile ($\varepsilon = 35.69$), methanol ($\varepsilon = 32.61$), dichloromethane ($\varepsilon = 8.93$), toluene ($\varepsilon = 2.37$) and cyclohexane ($\varepsilon = 2.02$). Geometries were considered fully optimized when both the force (maximum and RMS force, 0.000450 and 0.000300 hartree bohr^{-1} thresholds, respectively) and displacement (maximum and RMS displacement, 0.0018 and 0.0012 bohr thresholds, respectively) values for all atoms were below the threshold criteria. All optimized geometries were checked to be true minima, by computing vibrational frequencies and checking they were all positive. Harmonic vibrational analysis for IR and Raman spectra were also performed and presented employing the B3LYP/6-31+G(d,p) theory level with no further scaling. Excited state properties were computed through the linear response-time dependent DFT (TD-DFT) formalism.[88–90] For the acid-base speciation, the pK_a values have been estimated by solving Equation (1):

$$pK_a^{calc} = m\Delta G_{S(BA)} + C_0 \quad (1)$$

where $\Delta G_{S(BA)}$ is the Gibbs free energy difference between the acid (A) and the corresponding conjugated basic form (B) in aqueous solution, m and C_0 are calculated according to the previously published parameters fitting.[91] The molar fractions of the neutral and anionic form of each squaraine herein reported, is evaluated at pH = 7.4, according to the methodology and the computational protocol hitherto proposed.[92] Briefly, these calculations were performed by using the Minnesota M05-2X[93] hybrid functional in combination with 6-31+G(d,p) basis set and by employing the SMD solvation model.[94]

III. RESULTS AND DISCUSSION

A. Conformations and Protonation States

We first studied the structural diversity that **SQ**, **DPSQ**, and **DBSQ** might exhibit in solution at room temperature. Understanding the factors leading to such distortions is crucial for predicting the stability and reactivity of these molecules under various conditions. The relevance of three distinct structural forms (see their graphical representations for **SQ** in Figure S1) are investigated: planar (*p*-), distorted (*d*-), and mono-anionic (*a*-), the latter arising from an acid-base equilibrium. The planar structure (*p*-) reflects a symmetrical arrangement (belonging to the D_{2h} point group) of atoms within the squaraine molecules and it is stabilized by a network of 4 intramolec-

ular hydrogen bonds. The presence of these bonds contributes to the overall symmetry of the structure and underlines the importance of both intramolecular forces in maintaining a particular conformational state and intermolecular interactions (i.e. with protic solvents) in perturbing such conformation. The distorted structure (*d*-), on the other hand, suggests deviations from the higher symmetric conformation, hinting at potential distortions in the molecular geometry due to thermal fluctuations and solvent polarity. This conformation is particularly interesting given its potential implications on the electronic and vibrational properties of the compounds (i.e. absorption band shape). Distorted squaraines show a reduced number of intramolecular hydrogen bonds (reduced to 2) leading to a significant alteration in the internal forces that stabilize the molecular structure. A key feature of this distortion is the rotation or twisting of the C–C bonds between the squaric and phenolic carbon atoms. The degree of distortion is quantified by an approximate rotation angle of 30 degrees, as illustrated in Figure S1. Finally, the mono-anionic structure (*a*-), arising from an acid-base equilibrium, adds another layer of complexity to the conformational landscape of squaraines. This anionic form also is not planar and may exhibit distinct electronic and spectroscopic properties compared to its neutral counterparts, opening up avenues for exploring the impact of charged species on the electronic and vibrational behavior of these molecules (see next paragraphs). The susceptibility of squaraines to environment-induced and thermally-driven distortions is not merely an empirical observation; it could held significant implications for their use in technological applications.

B. Vibrational Analysis: Infrared and Raman Spectra

Vibrational analysis of **SQ**, **DPSQ** and **DBSQ** conformations has been carried in acetonitrile solution and starting from the highly symmetrical (point group D_{2h}) and planar geometrical guess for all squaraines, obtaining the corresponding minimum energy structures via the geometry optimization procedure (see Materials and Methods section for further details). Both IR and Raman spectra of **SQ**, **DPSQ** and **DBSQ** dyes were computed (for the planar conformation) and experimentally measured. We wish to stress that although IR and Raman spectra were experimentally collected in solid phase and vibrational analysis was performed in solution this comparisons can help in highlighting the main vibrational features of such systems. Resulting minimum structures are all planar; **SQ** and **DPSQ** belong to a final C_{2h} and **DBSQ** to a final C_2 point groups, respectively and their optimized structures are reported in Figure 1.

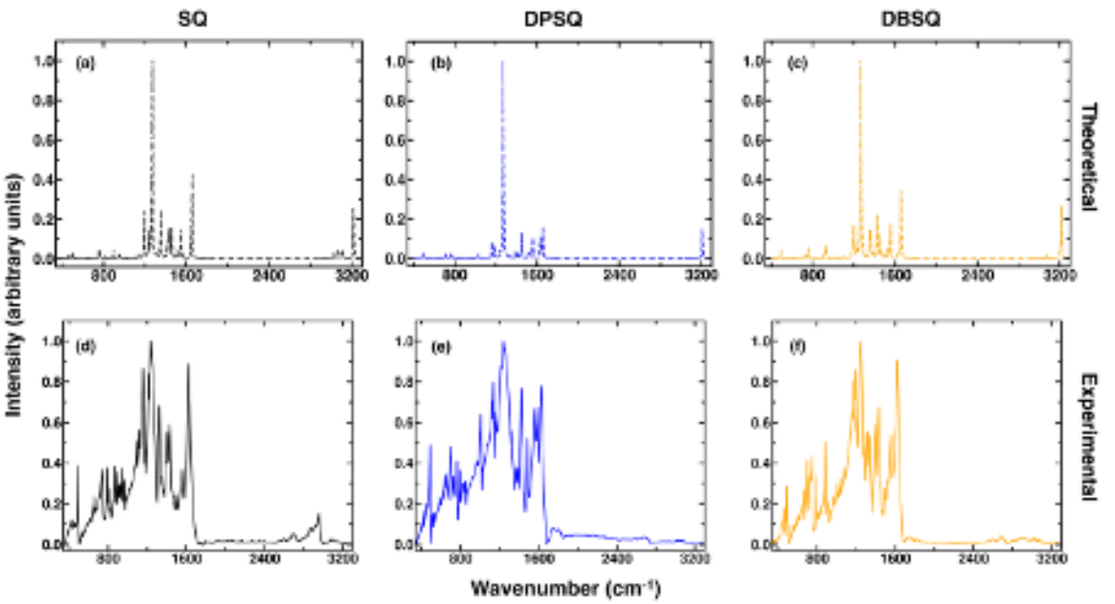

FIG. 2. Infrared spectra. Top panels: B3LYP/6-31+G(d,p)/C-PCM in acetonitrile solution (half width at half maximum is 4 cm^{-1}), *p*-**SQ** dashed black line **(a)**, *p*-**DPSQ** dashed blue line **(b)** and *p*-**DBSQ** dashed orange line **(c)**. Bottom panels: Experiments in solid-state (see Materials and Methods section for further details), **SQ** solid black line **(d)**, **DPSQ** solid blue line **(e)** and **DBSQ** solid orange line **(f)**, in the 340 cm^{-1} to 3300 cm^{-1} wavenumber range. The experimental spectra have been corrected to remove scattering contributions. Intensities have been renormalized for a better comparison.

Computed infrared spectra of planar (*p*-) **SQ**, **DPSQ** and **DBSQ** are first compared with the experiments and reported in Figure 2. Collective/backbone modes are found in the $\sim 1100 - 1750$ cm^{-1} energy range for all studied squaraines, such modes are asymmetric and symmetric stretching of C–C, C–O and C–N bonds. In particular, in this spectral region the most intense mode results in a ring breathing of both phenolic rings and is located at ~ 1250 cm^{-1} (see Figure S5 for *p*-**DPSQ**). As expected, at higher energies, above 3000 cm^{-1}, O–H and C–H stretching modes appear. Thus, we present the vibrational analysis of distorted (*d*-) and anionic (*a*-) conformations for the investigated **SQ** squaraine (**SQ** conformations are displayed in Figure S1). Such analysis is focused on the collective/backbone modes frequency range ($1000 - 1800$ cm^{-1}) and reported in Figure 3. By reducing the overall symmetry of the squaraine, the resulting configurations (both distorted and anionic) have more active vibrational modes in the $\sim 1100 - 1750$ cm^{-1} frequency range. The computed most intense vibrational mode is very sensitive to the conformation and protonation. Indeed, the aromatic ring breathing mode of planar **SQ** is found at ~ 1250 cm^{-1} (see Figure S4

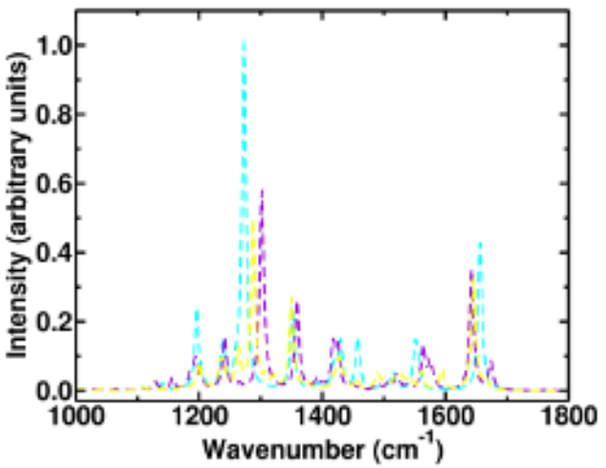

FIG. 3. B3LYP/6-31+G(d,p)/C-PCM infrared spectra of different conformations and protonation states in acetonitrile solution. *p*-**SQ** dashed cyan line, *d*-**SQ** dashed violet line and *a*-**SQ** dashed yellow line. 1000 cm^{-1} to 1800 cm^{-1} wavenumber range. Intensities were scaled with respect to the planar conformation which is the most intense. Half width at half maximum is 4 cm^{-1}.

for its representation), while in the anionic form and the distorted conformation a clear blueshift and a lowered intensity of such a band were found (see Figure 3, violet and yellow peaks at $\sim 1250\,\mathrm{cm}^{-1}$). We also noticed that in the $1400-1600\,\mathrm{cm}^{-1}$ spectral region (see Figure 3) all the analyzed conformations of **SQ** have unique infrared fingerprints due to the lowering of symmetry for distorted and anionic **SQ** (see Figure S6). As mentioned before, such collective modes mostly affect C–C, C–H and C–O on the squaric and phenolic residues. For *d*-**SQ** at $\sim 1560\,\mathrm{cm}^{-1}$ is a phenolic ring breathing (affected by the distortion) combined with two squaric C=O stretchings, while for *p*-**SQ** mainly affects the two squaric C=O bonds and O–H bending modes, and disappears for *a*-**SQ**. This analysis confirms that vibrational spectroscopy could help the study of the conformational and protonation equilibria in solution. With this in mind, the presented experimental IR spectra seem to better highlight the presence of the planar squaraines, although the **DPSQ** (panel **(e)** in Figure 3) shows a broader peak in the most intense region $\sim 1250\,\mathrm{cm}^{-1}$, indicating a possible larger contribution of the other forms.

As additional analysis, we also report in Figure 4 the computed Raman spectra of the planar squaraines compared with experimental ones. This time the low frequency region is more active if compared to the IR spectra. In particular, *p*-**DPSQ** (computed spectrum, **(b)**, Figure 4) has an intense Raman mode at 1411 cm^{-1} which is a collective mode involving the breathing of phenolic

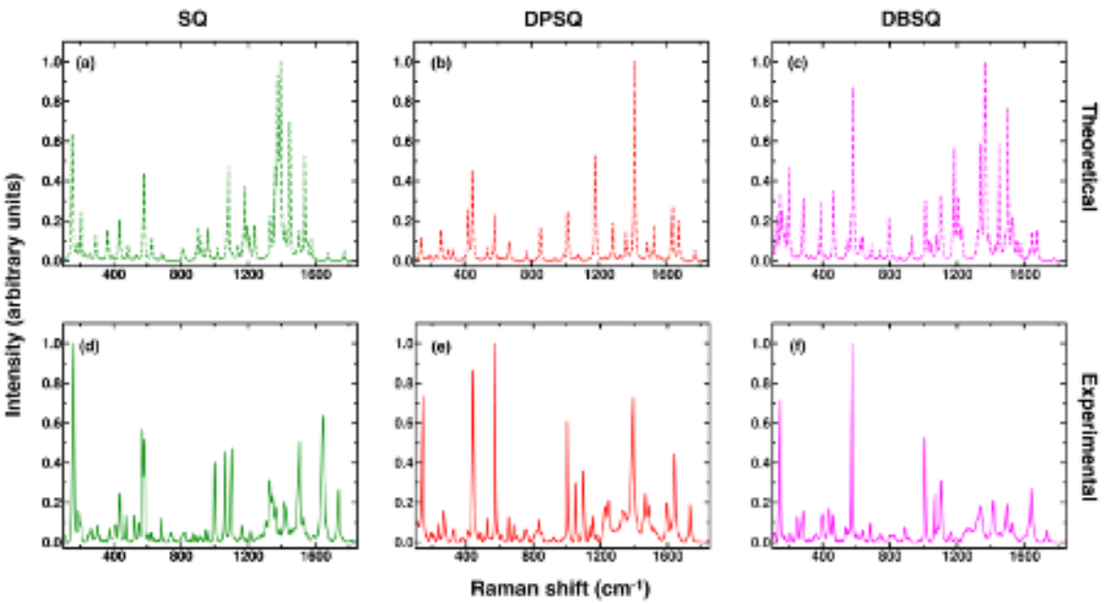

FIG. 4. Raman spectra. Top panels: B3LYP/6-31+G(d,p)/C-PCM in acetonitrile solution (half width at half maximum is $4\,\mathrm{cm}^{-1}$) *p*-**SQ** dashed green line **(a)**, *p*-**DPSQ** dashed red line **(b)** and *p*-**DBSQ** dashed magenta line **(c)**. Bottom panels: Experiments in solid-state (see Materials and Methods section for further details) **SQ** solid green line **(d)**, **DPSQ** solid red line **(e)** and **DBSQ** solid magenta line **(f)**. $100\,\mathrm{cm}^{-1}$ to $1850\,\mathrm{cm}^{-1}$ wavenumber range. Intensities have been renormalized for a better comparison.

fragments and symmetrical O–H stretching of hydroxyl groups engaged in hydrogen bonds with squaric oxygen atoms (Figure S8). Such mode is not found in planar **SQ** and **DBSQ**. By inspecting both IR (**(a)**, Figure 3) and Raman (**(a)**, Figure 4) spectra of *p*-**SQ** on the 1000 to $1800\,\mathrm{cm}^{-1}$ region, it has been found that in the range $1360 - 1420\,\mathrm{cm}^{-1}$ many collective modes that involve C–H and C–C motions on the N,N'-isobutyl substituents (Figure S7) appear.

Squaraine planar-distorted equilibrium is essentially important in solution due to the low energy barrier ($\sim -13\,\mathrm{kcal\,mol}^{-1}$) and this could result in a mediated spectrum between the forms. Although very useful for underlining the main vibrational features of such compounds, a quantitative analysis of the different contributions of conformations and protonation states on the experimental vibrational spectra obtained in solid phase is not straightforward. Thus, we further investigate the conformational and environment effects on the electronic properties via UV-Vis absorption in solution (see next paragraphs).

C. Electronic Properties: UV-Vis and Solvatochromism

1. Gauging the Theory Level

Previous computational studies on electronic absorption of similar squaraines have employed linear response TD-DFT and wave-function based methods.[55,95–99] In particular, it was proved that TD-DFT is reliable, although it can generally provide a consistent overestimation of the vertical transition energies[100,101] yielding to blueshifted λ_{max} due to the cyanine character of the excited states.[102] Despite the aforementioned issue, hybrid exchange-correlation functionals (e.g. the Minnesota hybrid functional M06[61]) can estimate the cyanine-charge transfer character of excited states of squaraines with a reasonable agreement with experimental optical data.[103–105]

In this section we report the extensive investigation of the accuracy of different theory levels, rooted in the DFT framework, for describing the optical properties of the squaraine dyes here studied. Thus, we analyzed the systems in their neutral and planar conformations by performing TD-DFT calculations and comparing the resulting vertical excitation energies (VEEs) with the maximum of the experimental UV-Vis absorption measured in acetonitrile solution. In all analyzed theory levels (see Materials and Methods section for further details), the first UV-Vis peak corresponds to a HOMO to LUMO transition that is described by an electronic density reorganization mostly localized on both phenolic rings, bound to the squaric residue, with an additional non negligible partial charge transfer (CT) from the ketonic oxygen atoms (squaric fragment) to the hydroxyl oxygen atoms (phenolic residues). The HOMO and LUMO representations for all analyzed squaraine dyes are reported in Figure S9. In the following analysis, all structures were optimized at the corresponding theory level and calculations are performed in acetonitrile solution (see Materials and Methods section).

TABLE I. TD-DFT accuracy analysis in acetonitrile solution. Experimental $\nu_{max,exp}$ (first column) and $\Delta\nu_{max}$ (VEE $-\ \nu_{max,exp}$) comparison for **SQ**, **DPSQ** and **DBSQ**. Results are reported in eV. All structures were optimized at the corresponding theory level by employing the 6-31+G(d,p) basis set.

	Exp	B3LYP	CAM-B3LYP	PBE0	M06	M06-2X	HSE06
SQ	1.92	+0.30	+0.38	+0.36	+0.35	+0.34	+0.35
DPSQ	1.90	+0.13	+0.33	+0.17	+0.23	+0.25	+0.12
DBSQ	1.94	+0.31	+0.38	+0.37	+0.36	+0.34	+0.36

First, we analyzed the basis set effect by employing the planar **DPSQ** and using the B3LYP functional and comparing the resulting VEEs computed by using the 6-31+G(d,p), 6-311+G(2d,p) and 6-311++G(2d,p)). There are no significant improvements increasing the size of the basis (see Table S2) and we used the 6-31+G(d,p) basis set for all subsequent calculations. Then, we checked the effect of including (or not) the corrections of the empirical dispersion, by using the D3 version of Grimme's dispersion with the original D3 damping function[106]. Also this time, we noticed no significant changes in the geometries, IR spectrum and the resulting VEEs (by employing the planar **DPSQ** and using the B3LYP functional with D3 and with no D3 corrections, see Figures S2 and S3 and Tables S1 and S2). From now on, the accuracy of different functionals has been gauged with the 6-31+G(d,p) basis set without taking into account the empirical dispersion corrections. Finally, we checked the VEEs using the B3LYP, PBE0, M06, M06-2X, CAM-B3LYP, and HSE06 (see Materials and Methods section for further details). In Table I the accuracy of each DFT kernel is summarized by reporting the error with respect to the corresponding experimental value. All the deployed functionals reproduce the same optical trend (red- or blueshift) on the $\nu_{\max}$ for the squaraines ($\nu_{\max,\mathbf{DBSQ}} > \nu_{\max,\mathbf{SQ}} > \nu_{\max,\mathbf{DPSQ}}$). As expected, all functionals show blueshifted values with respect to experimental measurements, but not always in a systematic way. In Figure S10 we report the TD-DFT predicted values against the experimental ones to better analyze the results and understand which functional is more accurate for describing the electronic transitions of the selected squaraines. **SQ** and **DBSQ** seems to show consistent errors among all analyzed functionals, while the computed values for **DPSQ** present a more complicated behavior, where only the Minnesota (M06 and M06-2X) and the long-range corrected (CAM-B3LYP) hybrid functionals perform more consistently as for the previous systems (errors of ~ 0.3 eV). As reported in Table I and through the analysis of Figure S10, we found that CAM-B3LYP is the best suitable functional in terms of consistent error, providing also the higher R^2 value (0.91, see also Table S3 in the ESI) among the DFT functionals. Thus, in the following computation of the electronic transitions and absorption spectra analysis we used the (TD-)CAM-B3LYP/6-31+G(d,p)/C-PCM, also because CAM-B3LYP is proven to be more reliable for describing charge transfer excitations (present in the anionic species, see next paragraphs).[107–114]

2. Influence of Conformational and Acid-Base Equilibria on UV-Vis Spectra

In this section, the possible influence of acid-base and conformation equilibria on the UV-Vis absorption spectrum of **SQ**, **DPSQ** and **DBSQ** has been analyzed. We wish to recall here that the vibrational analysis (see Section III B) confirmed that planar squaraines are more stable in energy ($\sim -13\,\mathrm{kcal\,mol^{-1}}$, averagely) than distorted ones. Thus, UV-Vis spectra of planar (*p*-), distorted (*d*-) and anionic (*a*-) squaraines in acetonitrile are reported in Figure 5. Here and in the following discussion, all TD-DFT computed values for each conformation and protonation states were shifted so that the VEE of the planar neutral conformation for each squaraine variant can match the experimental maximum absorption (see caption of Figure 5 for the applied corrections and Table S4 for raw VEEs values).

The experimental absorption spectra of all three squaraine dyes show a characteristic absorption band in the near-IR region between 600 nm and 700 nm. More specifically, **SQ**, **DPSQ** and **DBSQ** present a maximum absorption peak at 647 nm, at 654 nm and at 638 nm, respectively. The spectra of **SQ** and **DBSQ** have a shoulder at lower wavelengths, 594 nm and 588 nm, respectively, which so far has been mainly attributed to vibronic coupling.[115] The bandwidth of the absorption band of **DPSQ** is significantly wider than the ones of **SQ** and **DBSQ**, and consequently the higher energy shoulder is barely detectable. This might suggest the presence of more complex equilibria in solution for this molecular variant. We found that planar and distorted conformations have only one intense electronic excitation in the visible range, the HOMO to LUMO transition (MO isosurfaces are reported in Figure S11). By varying the squaraine conformation/protonation we noted that the corresponding excitation (see red and blue vertical lines in Figure 5) blueshifts and is less intense with respect to the non-distorted squaraine. Such transitions are found at ~ 646 nm and ~ 608 nm for planar and distorted **SQ**, respectively. For *p*- and *d*-**DPSQ**, the electronic transitions are found at ~ 651 nm and ~ 600 nm, while *p*- and *d*-**DBSQ** transitions lie around 640 nm and 599 nm. On the other hand, mono-anionic species present two bright electronic transitions (blue lines in Figure 5) in the visible range, found at ~ 579 nm and ~ 500 nm for anionic **SQ**. A similar trend was found also for anionic **DPSQ** and **DBSQ**. These two allowed electronic transitions are mostly due to the HOMO to LUMO (most intense) and HOMO-1 to LUMO (least intense, higher energy) excitations, although multiple contributions of other MO pairs are found for this last one. Thus we reported for a better analysis the hole-electron natural transition orbital (NTO) pairs[116] (for *a*-**SQ** in Figure S12, *a*-**DPSQ** and *a*-**DBSQ** in Figures S13 and S14). This second transition is

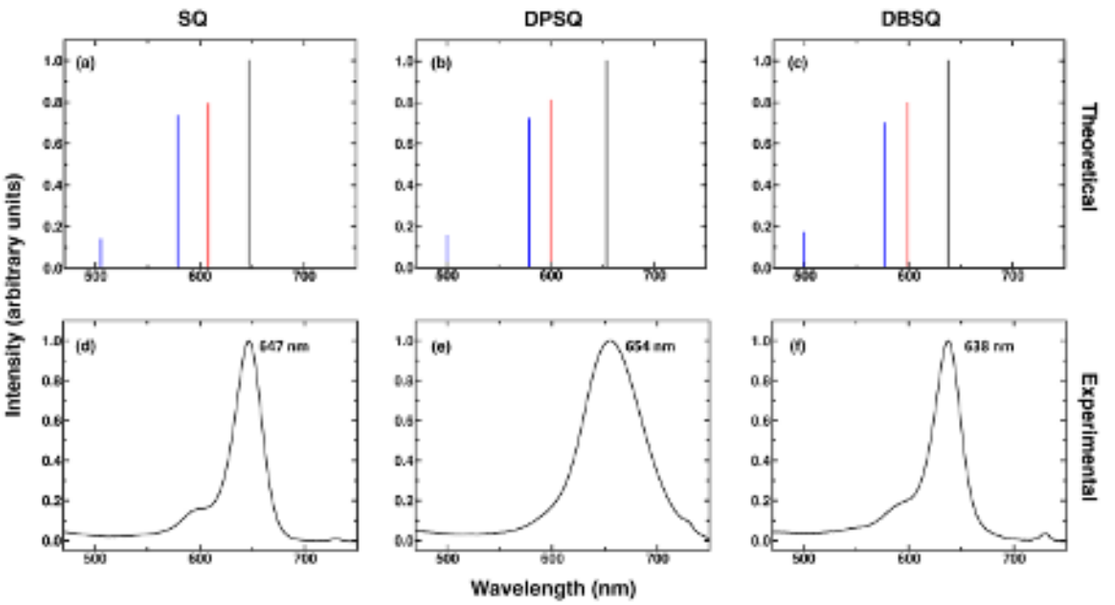

FIG. 5. UV-Vis spectra in acetonitrile solution. Top panels: TD-CAM-B3LYP/6-31+G(d,p)/C-PCM, *p*- (black), *d*- (red) and *a*- (blue) of **SQ**, **(a)**, **DPSQ**, **(b)** and **DBSQ**, **(c)**. Bottom panels: Experiments (see Materials and Methods section for further details), **SQ** solid black line **(d)**, **DPSQ** solid black line **(e)** and **DBSQ** solid black line **(f)**. TD-DFT VEEs for all conformations of each systems were uniformly shifted so that the planar neutral squaraine for each system can be better compared with the experimental maximum absorption (**SQ**, $\Delta\nu_{\mathrm{corr}}^{\mathrm{max}} = -0.38\,\mathrm{eV}$; **DPSQ**, $\Delta\nu_{\mathrm{corr}}^{\mathrm{max}} = -0.33\,\mathrm{eV}$; **DBSQ**, $\Delta\nu_{\mathrm{corr}}^{\mathrm{max}} = -0.38\,\mathrm{eV}$, see also Table I). 470 nm to 750 nm wavelength range. Theoretical intensities were scaled with respect to the planar conformation which gives the most intense electronic transition. Absolute VEEs frequency and oscillator strength values (not shifted and not scaled) for all squaraines in their different conformations and protonation states are summarized in Table S4.

a charge transfer excitation given by the distorted structure of the anionic squaraines, that becomes bright due to deprotonation (see hole-electron orbital pairs for all anionic squaraines in Figures S12 to S14, lower panels). Based on the observations in the experimental spectrum of **DPSQ** (see **(b)** and **(e)** panels in Figure 5), it is evident that this squaraine possesses a larger bandwidth. This could be attributed not only to the thermal and vibro-electronic broadening resulting from distorted conformations, but also to the presence of anionic deprotonated state of **DPSQ**, which is likely contributing to a wider absorption band in comparison to **SQ** and **DBSQ**. The experimental spectrum of a basified solution of **DPSQ** (Figure S16) confirms the presence of a blueshifted

band peaking at about 570 nm. To support this hypothesis, acid-base equilibria of **SQ**, **DPSQ** and **DBSQ** were computed both in water and acetonitrile solution for the phenolic proton to identify their predominant protonation states (see Figure S15 and Table S5). pK_a values around 9 have been obtained in water for **SQ** and **DBSQ** ($pK_a = 9.66$ and 9.14, respectively) while a pK_a value of 8.42 has been computed for **DPSQ**. As main result we found that the neutral form is always the most populated one for all the investigated systems. However, only for **DPSQ**, the molar fraction of the monoanionic species at pH = 7.4 could be considered not-negligible ($\sim 9\,\%$). In the acetonitrile solution, the molar fraction of anionic forms become smaller in all the cases. As final conclusion, we can say that for **SQ** and **DBSQ** the monoanionic form can be excluded, while for the **DPSQ** variant a non-negligible contribution of both asymmetric conformations and anionic species can be more important in the visible absorption in polar solvents (i.e. water, methanol) given the larger π-conjugation that the N-phenyl substituents can provide for this one for stabilizing the negative charge.

3. Solvatochromic Effects

In this last paragraph, the solvatochromic effect on the UV-Vis absorption spectrum for the inquired squaraines is studied. The absorption spectra of **DPSQ** was measured in several solvents of different polarity and the results are summarized in Table II. Then, we computed the solvatochromic shift (using the VEEs in different solvent) for all the systems and we reported the results in Figure 6.

TABLE II. Measured solvatochromic effect of **DPSQ**. $\nu_{max,exp}$, in eV and in parenthesis $\lambda_{max,exp}$, in nm.

Solvent	$\nu_{max,exp}$ ($\lambda_{max,exp}$)
Acetonitrile	1.90 (654)
Methanol	1.87 (663)
Dichloromethane	1.84 (673)
Toluene	1.83 (676)
Cyclohexane	1.83 (677)

It is clear that by increasing the solvent polarity the ν_{max} increases, ranging from 1.83 eV in cyclohexane, to 1.90 eV in acetonitrile. Such result are well reproduced in our calculations for the **DPSQ** and we predict a similar solvatochromic effect also for the other two systems (see

Tables S6 to S8). We have found that the predicted methanol values are the ones that deviate the most from the linear trend with solvent polarity (see Tables S6 to S8), given the protic nature of this solvent that requires an explicit treatment of the first shell interactions at least to have a better accuracy.[114,117] Additionally, we observed that **DPSQ** $\nu_{max,th}$ values better correlate with the solvent polarity with respect to the other squaraines (R^2 values for the linear regression: 0.88 for **DPSQ** and $\sim$0.8 for both **SQ** and **DBSQ**).

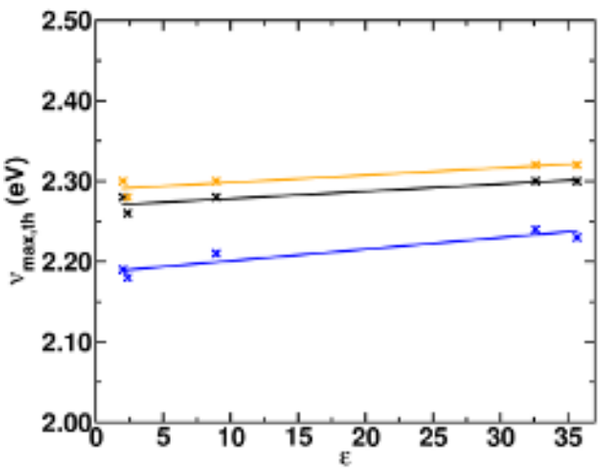

FIG. 6. TD-CAM-B3LYP/6-31+G(d,p)/C-PCM $\nu_{max,th}$ (computed as VEEs, where this time the absolute VEEs were used without further shifting, see Tables S6 to S8) vs. solvent dielectric constants. *p*-**SQ**, black; *p*-**DPSQ**, blue and *p*-**DBSQ**, orange. Trendlines are displayed. Corresponding dielectric solvent constants (ε) values are found in Materials and Methods section.

IV. CONCLUSIONS

A combined experimental and computational study was conducted for a comprehensive investigation of the effects of environment (solvent, pH) and conformations on the vibrational and electronic properties of symmetrically functionalized squaraine dyes. DFT, TD-DFT computational techniques combined with UV-Vis, Raman and IR measurements were here employed for this aim. Our analysis revealed that these compounds can exhibit different conformations (planar vs distorted) and protonation states (neutral vs anionic). The planar conformation is the most stable in non protic solvents (i.e. acetonitrile), due to the symmetrical arrangements of intramolecular hydrogen bonds, highlighting the significance of intermolecular interactions in tuning such conformational equilibrium and spectroscopic properties. Solvatocromism has been previously explained

in terms of peculiar behavior of quadrupolar dyes in terms of essential state models and vibronic couplings that might be influenced also by the solvent[36–38]. In this work, using quadrupolar dyes that have significant intramolecular hydrogen bond networks, we observed that the conformational equilibrium could also play a crucial role as well, since it is strongly affected by the solvent polarity. Distorted structures displayed deviations from higher symmetric conformations, with notable alterations in the molecular internal orientation, particularly in the rotation or twisting of C–C bonds. These distortions, which are accompanied by a reduction in intramolecular hydrogen bonds, can affect the electronic and vibrational properties of squaraine compounds. Squaraines are often used as dyes in devices such as DSSC, where they come into contact with solvents, gels or can form aggregates. Understanding the effects of these interactions can provide insight into the potential impact of the environment on their photophysics in the framework of several technological applications, including sensitizers, sensors, phototherapy and bioimaging[118]. Furthermore, the mono-anionic structure, resulting from an acid-base equilibrium, presented distinct electronic and spectroscopic properties compared to neutral counterparts, with a blueshifted absorption and the emergence of a higher energy and allowed charge transfer excitation. Vibrational analysis provided insights into the collective and backbone modes of squaraines, revealing distinctive spectral fingerprints for different conformations and protonation states. By comparing computed and experimental spectra, we elucidated the contributions of various conformations to the observed vibrational features, highlighting the impact of symmetry alterations on IR and Raman spectra. Our findings underline the importance of considering vibronic couplings, conformational diversity, acid-base equilibria, and solvent interactions in understanding the optical and structural properties of squaraine dyes in different environments. Protic and/or polar solvent might influence the most such conformational and protonation equilibria and we wish to analyze such effects in future studies. This study contributes to advancing the understanding of squaraine photophysics, providing valuable insights for the design and optimization of these molecules for the design and optimization of squaraine-based DSSCs devices.

SUPPLEMENTARY MATERIAL

B3LYP/6-31+G(d,p)/C-PCM in acetonitrile solution minimum energy structures of neutral planar, neutral distorted and anionic **SQ**; B3LYP/6-31+G(d,p)/C-PCM in acetonitrile solution minimum energy structure of neutral planar **DPSQ** with numbered atoms; B3LYP/6-31+G(d,p)/C-

PCM acetonitrile and B3LYP/6-31+G(d,p)/C-PCM acetonitrile/GD3 *p*-**DPSQ** minimum energy structure parameters and the resulting dipole moment comparison; Infrared spectra comparison of B3LYP/6-31+G(d,p)/C-PCM acetonitrile and B3LYP/6-31+G(d,p)/C-PCM acetonitrile/GD3 *p*-**DPSQ**; Representation of infrared and Raman mode displacement vectors for the vibrations of interest for the investigated squaraines; MO and NTO isosurfaces of the studied neutral planar, neutral distorted and anionic squaraines; Basis set and DFT kernel benchmarks; Computed VEE values for all squaraines in their different conformations and protonation states; Computed pk_a values of neutral planar squaraines in water and acetonitrile and molar fraction behaviours of neutral planar and anionic squaraines; Experimental UV-Vis spectrum of **DPSQ** at pH ~ 9; Computed solvatochromic effect on the first VEE for the neutral planar squaraines. List of the Cartesian coordinates of the CAM-B3LYP/6-31+G(d,p)/C-PCM (acetonitrile) minimum energy structures of the neutral planar, neutral distored and anionic squaraines. List of Cartesian coordinates of the B3LYP/6-31+G(d,p)/C-PCM (acetonitrile) and B3LYP/6-31+G(d,p)/C-PCM (acetonitrile)/GD3 minimum energy structures of the neutral planar squaraines.

ACKNOWLEDGMENTS

E.C. acknowledges financial support from the Ministero dell'Università e della Ricerca through the Project NEST-Spoke 9, code PE0000021 (CUP C93C22005230007). A.P. thanks the Italian Ministry of University and Research (projects: PRIN 202082CE3T_002), the University of Napoli Federico II (project: FRA-CosmoHab, CUP E65F22000050001) and Gaussian Inc. for financial support and IBiSCo (Infrastructure for BIg data and Scientific COmputing) for high-performance computing resources. M.E.A. acknowledges the CINECA award under the ISCRA initiative, for the availability of high-performance computing resources and support (HyPS4DAT).

AUTHOR DECLARATIONS

Conflict of Interest

The authors have no conflicts to disclose.

Data Availability Statement

The data that support the findings of this study are available within the supplementary material and from the corresponding authors upon reasonable request.

Author Contributions

E. Buttarazzi: Computational data acquisition and formal analysis; computational methodology (equal); writing–original draft (equal); writing-review & editing (equal).

A. Inchingolo: IR and UV-Vis experimental data acquisition and formal analysis and experimental methodology (equal).

D. Pedron: Raman experimental data acquisition and formal analysis and experimental methodology (equal).

M. E. Alberto: Conceptualization (lead); formal analysis (equal); computational methodology (lead); writing–original draft (equal); writing-review & editing (equal).

E. Collini: Conceptualization (lead); formal analysis (equal); funding acquisition (lead); experimental methodology (lead); supervision (lead); writing–original draft (equal); writing-review & editing (equal).

A. Petrone: Conceptualization (lead); formal analysis (equal); funding acquisition (lead); computational methodology (lead); supervision (lead); writing–original draft (equal); writing-review & editing (equal).

REFERENCES

[1]G. A. Chamberlain, "Organic solar cells: A review," Sol. Energy Mater Sol. Cells **8**, 47–83 (1983).

[2]A. Hagfeldt, G. Boschloo, L. Sun, L. Kloo, and H. Pettersson, "Dye-sensitized solar cells," Chem. Rev. **110**, 6595–6663 (2010).

[3]S. Mekhilef, R. Saidur, and A. Safari, "A review on solar energy use in industries," Renew. Sust. Energ. Rev. **15**, 1777–1790 (2011).

[4]G. Li, R. Zhu, and Y. Yang, "Polymer solar cells," Nat. Photon **6**, 153–161 (2012).

[5]N. R. Moheimani and D. Parlevliet, "Sustainable solar energy conversion to chemical and electrical energy," Renew. Sust. Energ. Rev. **27**, 494–504 (2013).

[6]T. D. Lee and A. U. Ebong, "A review of thin film solar cell technologies and challenges," Renew. Sust. Energ. Rev. **70**, 1286–1297 (2017).

[7]J. Y. Kim, J.-W. Lee, H. S. Jung, H. Shin, and N.-G. Park, "High-efficiency perovskite solar cells," Chem. Rev. **120**, 7867–7918 (2020).

[8]M. Riede, D. Spoltore, and K. Leo, "Organic solar cells—the path to commercial success," Adv. Energy Mater. **11**, 2002653 (2021).

[9]S. R. Wenham and M. A. Green, "Silicon solar cells," Prog. Photovolt.: Res. Appl. **4**, 3–33 (1996).

[10]C. Battaglia, A. Cuevas, and S. De Wolf, "High-efficiency crystalline silicon solar cells: status and perspectives," Energy Environ. Sci. **9**, 1552–1576 (2016).

[11]M. Grätzel, "Dye-sensitized solar cells," J. Photochem. Photobiol. C **4**, 145–153 (2003).

[12]J. Gong, K. Sumathy, Q. Qiao, and Z. Zhou, "Review on dye-sensitized solar cells (dsscs): Advanced techniques and research trends," Renew. Sust. Energ. Rev. **68**, 234–246 (2017).

[13]A. B. Muñoz-García, I. Benesperi, G. Boschloo, J. J. Concepcion, J. H. Delcamp, E. A. Gibson, G. J. Meyer, M. Pavone, H. Pettersson, A. Hagfeldt, and M. Freitag, "Dye-sensitized solar cells strike back," Chem. Soc. Rev. **50**, 12450–12550 (2021).

[14]B. O'regan and M. Grätzel, "A low-cost, high-efficiency solar cell based on dye-sensitized colloidal tio2 films," Nature **353**, 737–740 (1991).

[15]B. S. Richards, D. Hudry, D. Busko, A. Turshatov, and I. A. Howard, "Photon upconversion for photovoltaics and photocatalysis: a critical review: focus review," Chem. Rev. **121**, 9165–9195 (2021).

[16]Z. Hu, J. Wang, X. Ma, J. Gao, C. Xu, K. Yang, Z. Wang, J. Zhang, and F. Zhang, "A critical review on semitransparent organic solar cells," Nano Energy **78**, 105376 (2020).

[17]F. Grifoni, M. Bonomo, W. Naim, N. Barbero, T. Alnasser, I. Dzeba, M. Giordano, A. Tsaturyan, M. Urbani, T. Torres, C. Barolo, and F. Sauvage, "Toward sustainable, colorless, and transparent photovoltaics: State of the art and perspectives for the development of selective near-infrared dye-sensitized solar cells," Adv. Energy Mater. **11**, 2101598 (2021).

[18]S. Carretero-Palacios, A. Jiménez-Solano, and H. Míguez, "Plasmonic nanoparticles as light-harvesting enhancers in perovskite solar cells: a user's guide," ACS Energy Lett. **1**, 323–331 (2016).

[19]S. Erten-Ela, K. Ocakoglu, A. Tarnowska, O. Vakuliuk, and D. T. Gryko, "Performance of zinc chlorophyll based molecules for dye sensitized solar cell," Dyes Pigm. **114**, 129–137 (2015).

[20]A. K. Arof and T. L. Ping, *Chlorophyll*, edited by E. Jacob-Lopez (IntechOpen, 2017) Chap. 7, pp. 105–121.

[21]S. Sreeja and B. Pesala, "Co-sensitization aided efficiency enhancement in betanin-chlorophyll solar cell," Mater. Renew. Sustain. Energy. **7** (2018).

[22]H. A. Maddah, V. Berry, and S. K. Behura, "Biomolecular photosensitizers for dye-sensitized solar cells: Recent developments and critical insights," Renew. Sust. Energ. Rev. **121**, 109678 (2020).

[23]C.-Y. Chien and B.-D. Hsu, "Optimization of the dye-sensitized solar cell with anthocyanin as photosensitizer," Sol. Energy **98**, 203–211 (2013).

[24]A. S. Polo, M. K. Itokazu, and N. Y. M. Iha, "Metal complex sensitizers in dye-sensitized solar cells," Coordin. Chem. Rev. **248**, 1343–1361 (2004).

[25]B. Bozic-Weber, E. C. Constable, and C. E. Housecroft, "Light harvesting with earth abundant d-block metals: Development of sensitizers in dye-sensitized solar cells (dscs)," Coordin. Chem. Rev. **257**, 3089–3106 (2013).

[26]C. Zafer, B. Gultekin, C. Ozsoy, C. Tozlu, B. Aydin, and S. Icli, "Carbazole-based organic dye sensitizers for efficient molecular photovoltaics," Sol. Energy Mater Sol. Cells **94**, 655–661 (2010).

[27]D. El-Sherbiny, H. Cheema, F. El-Essawy, A. Abdel-Megied, and A. El-Shafei, "Synthesis and characterization of novel carbazole-based terpyridyl photosensitizers for dye-sensitized solar cells (dsscs)," Dyes Pigm. **115**, 81–87 (2015).

[28]P. Naik, A. Planchat, Y. Pellegrin, F. Odobel, and A. V. Adhikari, "Exploring the application of new carbazole based dyes as effective p-type photosensitizers in dye-sensitized solar cells," Sol. Energy **157**, 1064–1073 (2017).

[29]L. Beverina and P. Salice, "Squaraine compounds: Tailored design and synthesis towards a variety of material science applications," Eur. J. Org. Chem. **2010**, 1207–1225 (2010).

[30]K. Ilina, W. M. MacCuaig, M. Laramie, J. N. Jeouty, L. R. McNally, and M. Henary, "Squaraine dyes: molecular design for different applications and remaining challenges," Bioconjugate Chem. **31**, 194–213 (2019).

[31]C. Qin, W.-Y. Wong, and L. Han, "Squaraine dyes for dye-sensitized solar cells: Recent advances and future challenges," Chem. Asian J. **8**, 1706–1719 (2013).

[32]J. He, Y. J. Jo, X. Sun, W. Qiao, J. Ok, T.-i. Kim, and Z. Li, "Squaraine dyes for photovoltaic and biomedical applications," Adv. Func. Mater. **31**, 2008201 (2021).

[33]S.-Y. Park, K. Jun, and S.-W. Oh, "The novel functional chromophores based on squarylium dyes," Bull. Korean Chem. Soc. **26**, 428–432 (2005).

[34]L. Hu, Z. Yan, and H. Xu, "Advances in synthesis and application of near-infrared absorbing squaraine dyes," RSC Adv. **3**, 7667–7676 (2013).

[35]A. T. Rösch, S. H. M. Söntjens, J. Robben, A. R. A. Palmans, and T. Schnitzer, "Rotational isomerism of an amide substituted squaraine dye: A combined spectroscopic and computational study," J. Org. Chem. **86**, 13100–13103 (2021).

[36]F. Terenziani, A. Painelli, C. Katan, M. Charlot, and M. Blanchard-Desce, "Charge instability in quadrupolar chromophores: Symmetry breaking and solvatochromism," J. Am. Chem. Soc. **128**, 15742–15755 (2006).

[37]C. Zheng, C. Zhong, C. J. Collison, and F. C. Spano, "Non-kasha behavior in quadrupolar dye aggregates: The red-shifted h-aggregate," J. Phys. Chem. C **123**, 3203–3215 (2019).

[38]D. Timmer, F. Zheng, M. Gittinger, T. Quenzel, D. C. Lünemann, K. Winte, Y. Zhang, M. E. Madjet, J. Zablocki, A. Lützen, J.-H. Zhong, A. De Sio, T. Frauenheim, S. Tretiak, and C. Lienau, "Charge delocalization and vibronic couplings in quadrupolar squaraine dyes," J. Am. Chem. Soc. **144**, 19150–19162 (2022).

[39]R. A. Beck, A. Petrone, J. M. Kasper, M. J. Crane, P. J. Pauzauskie, and X. Li, "Effect of surface passivation on nanodiamond crystallinity," J. Phys. Chem. C **122**, 8573–8580 (2018).

[40]A. Petrone, D. B. Williams-Young, D. B. Lingerfelt, and X. Li, "Ab initio excited-state transient raman analysis," J. Phys. Chem. A **121**, 3958–3965 (2017).

[41]E. Q. Chong, D. B. Lingerfelt, A. Petrone, and X. Li, "Classical or quantum? a computational study of small ion diffusion in ii–vi semiconductor quantum dots," J. Phys. Chem. C **120**, 19434–19441 (2016).

[42]J. Hafner, C. Wolverton, and G. Ceder, "Toward computational materials design: the impact of density functional theory on materials research," MRS Bull. **31**, 659–668 (2006).

[43]R. Beaulac, Y. Feng, J. W. May, E. Badaeva, D. R. Gamelin, and X. Li, "Orbital pathways for mn^{2+}-carrier $sp-d$ exchange in diluted magnetic semiconductor quantum dots," Phys. Rev. B **84**, 195324 (2011).

[44]P. J. Lestrange, P. D. Nguyen, and X. Li, "Calibration of energy-specific tddft for modeling k-edge xas spectra of light elements," J. Chem. Theory Comput. **11**, 2994–2999 (2015).

[45]J. Aarons, M. Sarwar, D. Thompsett, and C.-K. Skylaris, "Perspective: Methods for large-scale density functional calculations on metallic systems," J. Chem. Phys. **145**, 220901 (2016).

[46]A. Petrone, J. J. Goings, and X. Li, "Quantum confinement effects on optical transitions in nanodiamonds containing nitrogen vacancies," Phys. Rev. B **94**, 165402 (2016).

[47]G. Donati, D. B. Lingerfelt, A. Petrone, N. Rega, and X. Li, ""watching" polaron pair formation from first-principles electron–nuclear dynamics," J. Phys. Chem. A **120**, 7255–7261 (2016).

[48]N. Li, Z. Zhu, C.-C. Chueh, H. Liu, B. Peng, A. Petrone, X. Li, L. Wang, and A. K.-Y. Jen, "Mixed cation faxpea1–xpbi3 with enhanced phase and ambient stability toward high-performance perovskite solar cells," Adv. Energy Mater. **7**, 1601307 (2017).

[49]D. C. Gary, S. E. Flowers, W. Kaminsky, A. Petrone, X. Li, and B. M. Cossairt, "Single-crystal and electronic structure of a 1.3 nm indium phosphide nanocluster," J. Am. Chem. Soc. **138**, 1510–1513 (2016).

[50]D. C. Gary, A. Petrone, X. Li, and B. M. Cossairt, "Investigating the role of amine in inp nanocrystal synthesis: destabilizing cluster intermediates by z-type ligand displacement," Chem. Commun. **53**, 161–164 (2017).

[51]J. L. Stein, M. I. Steimle, M. W. Terban, A. Petrone, S. J. L. Billinge, X. Li, and B. M. Cossairt, "Cation exchange induced transformation of inp magic-sized clusters," Chem. Mater. **29**, 7984–7992 (2017).

[52]G. Donati, D. B. Lingerfelt, C. M. Aikens, and X. Li, "Molecular vibration induced plasmon decay," J. Phys. Chem. C **121**, 15368–15374 (2017).

[53]S. Xu, J. E. T. Smith, S. Gozem, A. I. Krylov, and J. M. Weber, "Electronic spectra of tris(2,2'-bipyridine)-m(ii) complex ions in vacuo (m = fe and os)," Inorg. Chem. **56**, 7029–7037 (2017).

[54]U. Raucci, M. G. Chiariello, F. Coppola, F. Perrella, M. Savarese, I. Ciofini, and N. Rega, "An electron density based analysis to establish the electronic adiabaticity of proton coupled electron transfer reactions," J. Comput. Chem. **41**, 1835–1841 (2020).

[55]F. Bassal, A. D. Laurent, B. Le Guennic, and D. Jacquemin, "Exploring the excited-states of squaraine dyes with td-dft, sos-cis (d) and adc (2)," Dyes Pigm. **138**, 169–175 (2017).

[56]M. J. Frisch, G. W. Trucks, H. B. Schlegel, G. E. Scuseria, M. A. Robb, J. R. Cheeseman, G. Scalmani, V. Barone, G. A. Petersson, H. Nakatsuji, X. Li, M. Caricato, A. V. Marenich, J. Bloino, B. G. Janesko, R. Gomperts, B. Mennucci, H. P. Hratchian, J. V. Ortiz, A. F. Izmaylov, J. L. Sonnenberg, D. Williams-Young, F. Ding, F. Lipparini, F. Egidi, J. Goings, B. Peng, A. Petrone, T. Henderson, D. Ranasinghe, V. G. Zakrzewski, J. Gao, N. Rega, G. Zheng, W. Liang, M. Hada, M. Ehara, K. Toyota, R. Fukuda, J. Hasegawa, M. Ishida, T. Nakajima, Y. Honda, O. Kitao, H. Nakai, T. Vreven, K. Throssell, J. A. Montgomery, Jr., J. E. Peralta,

F. Ogliaro, M. J. Bearpark, J. J. Heyd, E. N. Brothers, K. N. Kudin, V. N. Staroverov, T. A. Keith, R. Kobayashi, J. Normand, K. Raghavachari, A. P. Rendell, J. C. Burant, S. S. Iyengar, J. Tomasi, M. Cossi, J. M. Millam, M. Klene, C. Adamo, R. Cammi, J. W. Ochterski, R. L. Martin, K. Morokuma, O. Farkas, J. B. Foresman, and D. J. Fox, "Gaussian 16 Revision C.01," (2016), gaussian Inc. Wallingford CT.

[57]C. Lee, W. Yang, and R. G. Parr, "Development of the colle-salvetti correlation-energy formula into a functional of the electron density," Phys. Rev. B **37**, 785–789 (1988).

[58]B. Miehlich, A. Savin, H. Stoll, and H. Preuss, "Results obtained with the correlation energy density functionals of becke and lee, yang and parr," Chem. Phys. Lett. **157**, 200–206 (1989).

[59]A. D. Becke, "Density-functional thermochemistry. iii. the role of exact exchange," J. Chem. Phys. **98**, 5648–5652 (1993).

[60]C. Adamo and V. Barone, "Toward reliable density functional methods without adjustable parameters: The pbe0 model," J. Chem. Phys. **110**, 6158–6170 (1999).

[61]Y. Zhao and D. G. Truhlar, "The m06 suite of density functionals for main group thermochemistry, thermochemical kinetics, noncovalent interactions, excited states, and transition elements: two new functionals and systematic testing of four m06-class functionals and 12 other functionals," Theor. Chem. Acc. **120**, 215–241 (2008).

[62]T. Yanai, D. P. Tew, and N. C. Handy, "A new hybrid exchange-correlation functional using the coulomb-attenuating method (cam-b3lyp)," Chem. Phys. Lett. **393**, 51–57 (2004).

[63]J. Heyd, G. E. Scuseria, and M. Ernzerhof, "Hybrid functionals based on a screened coulomb potential," J. Chem. Phys. **118**, 8207–8215 (2003).

[64]J. Heyd and G. E. Scuseria, "Efficient hybrid density functional calculations in solids: Assessment of the heyd–scuseria–ernzerhof screened coulomb hybrid functional," J. Chem. Phys. **121**, 1187–1192 (2004).

[65]J. Heyd and G. E. Scuseria, "Assessment and validation of a screened coulomb hybrid density functional," J. Chem. Phys. **120**, 7274–7280 (2004).

[66]J. Heyd, J. E. Peralta, G. E. Scuseria, and R. L. Martin, "Energy band gaps and lattice parameters evaluated with the heyd-scuseria-ernzerhof screened hybrid functional," J. Chem. Phys. **123**, 174101 (2005).

[67]A. F. Izmaylov, G. E. Scuseria, and M. J. Frisch, "Efficient evaluation of short-range hartree-fock exchange in large molecules and periodic systems," J. Chem. Phys. **125**, 104103 (2006).

[68]A. V. Krukau, O. A. Vydrov, A. F. Izmaylov, and G. E. Scuseria, "Influence of the exchange screening parameter on the performance of screened hybrid functionals," J. Chem. Phys. **125**, 224106 (2006).

[69]T. M. Henderson, A. F. Izmaylov, G. Scalmani, and G. E. Scuseria, "Can short-range hybrids describe long-range-dependent properties?" J. Chem. Phys. **131**, 044108 (2009).

[70]R. Ditchfield, W. J. Hehre, and J. A. Pople, "Self-Consistent Molecular-Orbital Methods. IX. An Extended Gaussian-Type Basis for Molecular-Orbital Studies of Organic Molecules," J. Chem. Phys. **54**, 724–728 (1971).

[71]W. J. Hehre, R. Ditchfield, and J. A. Pople, "Self—Consistent Molecular Orbital Methods. XII. Further Extensions of Gaussian—Type Basis Sets for Use in Molecular Orbital Studies of Organic Molecules," J. Chem. Phys. **56**, 2257–2261 (1972).

[72]P. C. Hariharan and J. A. Pople, "The influence of polarization functions on molecular orbital hydrogenation energies," Theor. Chem. Acc. **28**, 213–222 (1973).

[73]P. Hariharan and J. Pople, "Accuracy of ah n equilibrium geometries by single determinant molecular orbital theory," Mol. Phys. **27**, 209–214 (1974).

[74]M. S. Gordon, "The isomers of silacyclopropane," Chem. Phys. Lett. **76**, 163–168 (1980).

[75]M. M. Francl, W. J. Pietro, W. J. Hehre, J. S. Binkley, M. S. Gordon, D. J. DeFrees, and J. A. Pople, "Self-consistent molecular orbital methods. XXIII. A polarization-type basis set for second-row elements," J. Chem. Phys. **77**, 3654–3665 (1982).

[76]G. A. Petersson, A. Bennett, T. G. Tensfeldt, M. A. Al-Laham, W. A. Shirley, and J. Mantzaris, "A complete basis set model chemistry. I. The total energies of closed-shell atoms and hydrides of the first-row elements," J. Chem. Phys. **89**, 2193–2218 (1988).

[77]R. C. Binning Jr. and L. A. Curtiss, "Compact contracted basis sets for third-row atoms: Ga–kr," J. Comput. Chem. **11**, 1206–1216 (1990).

[78]G. A. Petersson and M. A. Al-Laham, "A complete basis set model chemistry. II. Open-shell systems and the total energies of the first-row atoms," J. Chem. Phys. **94**, 6081–6090 (1991).

[79]J.-P. Blaudeau, M. P. McGrath, L. A. Curtiss, and L. Radom, "Extension of Gaussian-2 (G2) theory to molecules containing third-row atoms K and Ca," J. Chem. Phys. **107**, 5016–5021 (1997).

[80]V. A. Rassolov, J. A. Pople, M. A. Ratner, and T. L. Windus, "6-31G* basis set for atoms K through Zn," J. Chem. Phys. **109**, 1223–1229 (1998).

[81]V. A. Rassolov, M. A. Ratner, J. A. Pople, P. C. Redfern, and L. A. Curtiss, "6-31g* basis set for third-row atoms," J. Comput. Chem. **22**, 976–984 (2001).

[82]B. Mennucci and J. Tomasi, "Continuum solvation models: A new approach to the problem of solute's charge distribution and cavity boundaries," J. Chem. Phys. **106**, 5151–5158 (1997).

[83]V. Barone, M. Cossi, and J. Tomasi, "Geometry optimization of molecular structures in solution by the polarizable continuum model," J. Comput. Chem. **19**, 404–417 (1998).

[84]V. Barone and M. Cossi, "Quantum calculation of molecular energies and energy gradients in solution by a conductor solvent model," J. Phys. Chem. A **102**, 1995–2001 (1998).

[85]M. Cossi, N. Rega, G. Scalmani, and V. Barone, "Polarizable dielectric model of solvation with inclusion of charge penetration effects," J. Chem. Phys. **114**, 5691–5701 (2001).

[86]M. Cossi, G. Scalmani, N. Rega, and V. Barone, "New developments in the polarizable continuum model for quantum mechanical and classical calculations on molecules in solution," The Journal of Chemical Physics **117**, 43–54 (2002).

[87]M. Cossi, N. Rega, G. Scalmani, and V. Barone, "Energies, structures, and electronic properties of molecules in solution with the c-pcm solvation model," J. Comput. Chem. **24**, 669–681 (2003).

[88]M. E. Casida, *Recent Advances in Density Functional Methods*, edited by D. P. Chong (World Scientific, 1995) pp. 155–192.

[89]R. E. Stratmann, G. E. Scuseria, and M. J. Frisch, "An efficient implementation of time-dependent density-functional theory for the calculation of excitation energies of large molecules," J. Chem. Phys. **109**, 8218–8224 (1998).

[90]A. Dreuw and M. Head-Gordon, "Single-reference ab initio methods for the calculation of excited states of large molecules," Chem. Rev. **105**, 4009–4037 (2005).

[91]A. Galano and J. R. Alvarez-Idaboy, "A computational methodology for accurate predictions of rate constants in solution: Application to the assessment of primary antioxidant activity," J. Comput. Chem. **34**, 2430–2445 (2013).

[92]A. Galano, A. Pérez-González, R. Castañeda-Arriaga, L. Muñoz-Rugeles, G. Mendoza-Sarmiento, A. Romero-Silva, A. Ibarra-Escutia, A. M. Rebollar-Zepeda, J. R. León-Carmona, M. A. Hernández-Olivares, and J. R. Alvarez-Idaboy, "Empirically fitted parameters for calculating pka values with small deviations from experiments using a simple computational strategy," J. Chem. Inf. Model. **56**, 1714–1724 (2016).

[93]Y. Zhao, N. E. Schultz, and D. G. Truhlar, "Design of density functionals by combining the method of constraint satisfaction with parametrization for thermochemistry, thermochemical kinetics, and noncovalent interactions," J. Chem. Theory Comput. **2**, 364–382 (2006).

[94]A. V. Marenich, C. J. Cramer, and D. G. Truhlar, "Universal solvation model based on solute electron density and on a continuum model of the solvent defined by the bulk dielectric constant and atomic surface tensions," J. Phys. Chem. B **113**, 6378–6396 (2009).

[95]F. Meyers, C.-T. Chen, S. R. Marder, J.-L. Brédas, and F. Meyers, "Electronic structure and linear and nonlinear optical properties of symmetrical and unsymmetrical squaraine dyes," Chem. Eur. J. **3**, 530–537 (1997).

[96]A. D. Laurent, C. Adamo, and D. Jacquemin, "Dye chemistry with time-dependent density functional theory," Phys. Chem. Chem. Phys. **16**, 14334–14356 (2014).

[97]T. Geiger, S. Kuster, J.-H. Yum, S.-J. Moon, M. K. Nazeeruddin, M. Grätzel, and F. Nüesch, "Molecular design of unsymmetrical squaraine dyes for high efficiency conversion of low energy photons into electrons using tio2 nanocrystalline films," Adv. Funct. Mater. **19**, 2720–2727 (2009).

[98]A. D. Quartarolo, E. Sicilia, and N. Russo, "On the potential use of squaraine derivatives as photosensitizers in photodynamic therapy: a tddft and ricc2 survey," J. Chem. Theory Comput. **5**, 1849–1857 (2009).

[99]G. Barcenas, A. Biaggne, O. A. Mass, C. K. Wilson, O. M. Obukhova, O. S. Kolosova, A. L. Tatarets, E. Terpetschnig, R. D. Pensack, J. Lee, W. B. Knowlton, B. Yurke, and L. Li, "First-principles studies of substituent effects on squaraine dyes," RSC Adv. **11**, 19029–19040 (2021).

[100]D. J. Tozer, "Relationship between long-range charge-transfer excitation energy error and integer discontinuity in kohn–sham theory," J. Chem. Phys. **119**, 12697–12699 (2003).

[101]A. Dreuw and M. Head-Gordon, "Failure of time-dependent density functional theory for long-range charge-transfer excited states: The zincbacteriochlorin-bacteriochlorin and bacteriochlorophyll-spheroidene complexes," J. Am. Chem. Soc. **126**, 4007–4016 (2004).

[102]B. Le Guennic and D. Jacquemin, "Taking up the cyanine challenge with quantum tools," Acc. Chem. Res. **48**, 530–537 (2015).

[103]E. Ronchi, R. Ruffo, S. Rizzato, A. Albinati, L. Beverina, and G. A. Pagani, "Regioselective synthesis of 1,2- vs 1,3-squaraines," Org. Lett. **13**, 3166–3169 (2011).

[104]D. Jacquemin, B. Mennucci, and C. Adamo, "Excited-state calculations with td-dft: from benchmarks to simulations in complex environments," Phys. Chem. Chem. Phys. **13**, 16987–

16998 (2011).

[105]M. E. Alberto, G. Mazzone, A. D. Quartarolo, F. F. R. Sousa, E. Sicilia, and N. Russo, "Electronic spectra and intersystem spin-orbit coupling in 1,2- and 1,3-squaraines," J. Comput. Chem. **35**, 2107–2113 (2014).

[106]S. Grimme, J. Antony, S. Ehrlich, and H. Krieg, "A consistent and accurate ab initio parametrization of density functional dispersion correction (DFT-D) for the 94 elements H-Pu," J. Chem. Phys. **132**, 154104 (2010).

[107]F. Coppola, P. Cimino, F. Perrella, L. Crisci, A. Petrone, and N. Rega, "Electronic and vibrational manifold of tetracyanoethylene–chloronaphthalene charge transfer complex in solution: Insights from td-dft and ab initio molecular dynamics," J. Phys. Chem. A **126**, 7179–7192 (2022).

[108]R. Kobayashi and R. D. Amos, "The application of cam-b3lyp to the charge-transfer band problem of the zincbacteriochlorin–bacteriochlorin complex," Chem. Phys. Lett. **420**, 106–109 (2006).

[109]Z.-L. Cai, M. J. Crossley, J. R. Reimers, R. Kobayashi, and R. D. Amos, "Density functional theory for charge transfer: The nature of the n-bands of porphyrins and chlorophylls revealed through cam-b3lyp, caspt2, and sac-ci calculations," J. Phys. Chem. B **110**, 15624–15632 (2006).

[110]I. V. Rostov, R. D. Amos, R. Kobayashi, G. Scalmani, and M. J. Frisch, "Studies of the ground and excited-state surfaces of the retinal chromophore using cam-b3lyp," J. Phys. Chem. B **114**, 5547–5555 (2010).

[111]R. Li, J. Zheng, and D. G. Truhlar, "Density functional approximations for charge transfer excitations with intermediate spatial overlap," Phys. Chem. Chem. Phys. **12**, 12697–12701 (2010).

[112]H. Li, R. Nieman, A. J. A. Aquino, H. Lischka, and S. Tretiak, "Comparison of lc-tddft and adc(2) methods in computations of bright and charge transfer states in stacked oligothiophenes," J. Chem. Theory Comput. **10**, 3280–3289 (2014).

[113]F. Perrella, F. Coppola, N. Rega, and A. Petrone, "An expedited route to optical and electronic properties at finite temperature via unsupervised learning," Molecules **28**, 3411 (2023).

[114]F. Perrella, A. Petrone, and N. Rega, "Understanding charge dynamics in dense electronic manifolds in complex environments," J. Chem. Theory Comput. **19**, 626–639 (2023).

[115]R. Borrelli, S. Ellena, and C. Barolo, "Theoretical and experimental determination of the absorption and emission spectra of a prototypical indolenine-based squaraine dye," Phys. Chem.

Chem. Phys. **16**, 2390–2398 (2014).

[116]R. L. Martin, "Natural transition orbitals," J. Chem. Phys. **118**, 4775–4777 (2003).

[117]U. Raucci, F. Perrella, G. Donati, M. Zoppi, A. Petrone, and N. Rega, "Ab-initio molecular dynamics and hybrid explicit-implicit solvation model for aqueous and nonaqueous solvents: Gfp chromophore in water and methanol solution as case study," J. Comput. Chem. **41**, 2228–2239 (2020).

[118]K. Ilina, W. M. MacCuaig, M. Laramie, J. N. Jeouty, L. R. McNally, and M. Henary, "Squaraine dyes: Molecular design for different applications and remaining challenges," Bioconjugate Chem. **31**, 194–213 (2020).